Published in final edited form as:

Skeletal Radiol. 2019 December ; 48(12): 1999–2007. doi:10.1007/s00256-019-03241-w.

Motion Compensation in Extremity Cone-Beam Computed Tomography

Alejandro Sisniega[1], **Gaurav K Thawait**[1,2], **Delaram Shakoor**[2], **Jeffrey H. Siewerdsen**[1,2], **Shadpour Demehri**[2], **Wojciech Zbijewski**[1]

[1)]Department of Biomedical Engineering, Johns Hopkins University, Baltimore, MD,21205, USA

[2)]Russel H Morgan Department of Radiology, Johns Hopkins University, Baltimore, MD,21278, USA

Abstract

Objectives: To evaluate the improvement in extremity Cone-Beam Computed Tomography (CBCT) image quality in datasets with motion artifact using a motion compensation method based on maximizing image sharpness.

Methods: Following IRB approval, retrospective analysis of 308 CBCT scans of lower extremities was performed by a fellowship-trained musculoskeletal radiologist to identify images with moderate to severe motion artifact. Twenty-four scans of 22 patients (18 male, 4 female; mean 32 yo, ranging 21-74 yo) were chosen for inclusion. Sharp (bone) and smooth (soft-tissue) reconstructions were processed using the motion compensation algorithm. Two experts rated visualization of trabecular bone, cortical bone, joint spaces, and tendon on a 9-level Likert scale with and without motion compensation (a total of 96 datasets). Visual Grading Characteristics (VGC) was used to quantitatively determine the difference in image quality following motion compensation. Intra-class correlation coefficient (ICC) was obtained to assess inter-observer agreement.

Results: Motion-compensated images exhibited appreciable reduction in artifacts. The observer study demonstrated the associated improvement in diagnostic quality. The fraction of cases receiving scores better than “Fair” increased from less than 10% without compensation to 40% - 70% following compensation, depending on the task. The area under the VGC curve was 0.75 (tendon) to 0.85 (cortical bone), confirming preference for motion compensated images. ICC values showed excellent agreement between readers before (ICC range: 0.8-0.91) and after motion compensation (ICC range: 0.92-0.97).

Conclusion: The motion compensation algorithm significantly improved the visualization of bone and soft-tissue structures in extremity CBCT for cases exhibiting patient motion.

Keywords

Motion compensation; Extremity Cone-Beam CT; Visual Grading Characteristic; Weight-bearing

Please address all correspondence and reprint requests to: Baltimore, MD, 21205, USA. wzbijewski@jhu.edu, Telephone: 410-955-1319, Fax:.

This work has originated in Department of Biomedical Engineering, Johns Hopkins University, Baltimore, MD, 21205, USA

Introduction

Dedicated extremity cone-beam computed tomography (CBCT) has emerged as a unique imaging modality for assessment of musculoskeletal disorders [1-4]. CBCT uses a large-area flat-panel detector and a pyramid-shaped X-ray beam to acquire three-dimensional images in single rotation of scanner gantry. A single CBCT scan yields a volumetric field-of-view of approx. 20 cm^3 at high, isotropic spatial resolution. Extremity CBCT have been reported to provide sufficient contrast resolution for evaluation of menisci, ligaments and cartilage, and superior visualization of osseous structures compared to multi-detector CT (MDCT) at a lower radiation dose [5, 6]. Another unique feature of this modality is the ability to obtain images of the lower extremity under physiologic weight-bearing (WB), which could potentially add diagnostic value in management of certain pathologies involving WB joints such as the knee and the ankle [7, 8].

Despite these substantial advantages, images obtained from CBCT have some drawbacks, including higher conspicuous scatter artifacts and noise, which can be addressed by Monte Carlo model-based correction [9, 10] and application of statistical model-based reconstruction [11]. In addition, current CBCT scanner configurations [12] require longer scan time (20-30 seconds), compared to MDCT or radiography [6], which leads to increased occurrence of patient motion, particularly in weight-bearing imaging. Even though light immobilization is typically used in CBCT, it is not always effective. Compared to MDCT, CBCT image quality is thus challenged by motion artifacts that occur more frequently and are typically more severe [13]. Such artifacts include streaks arising from high contrast structures (e.g. bone/soft-tissue boundaries), double contours, and motion-induced blurring. We note that this paper uses the term “motion artifacts” (or simply “artifacts” when discussed in the context of motion / motion compensation) to denote the totality of those effects. Whenever we refer to other sources of image degradation (e.g. scatter), we include an appropriate qualifier with the word artifact.

We have developed a method for reducing motion artifacts based on a 3D “autofocus” algorithm that estimates patient motion directly from the scan data using an image sharpness criterion [14]. This method obviates the need for fiducial markers or tracking devices and can be applied retrospectively to motion-contaminated scans [15, 16]. Previous work showed successful compensation of motion artifacts in simulations, phantom studies, and qualitative evaluation in images of a single patient with moderate motion [14].

In this study, we intend to perform a rigorous observer study to test the hypothesis that a clinically relevant soft-tissue and bone imaging tasks benefit from motion compensation using the above mentioned algorithm. We first present a phantom experiment to illustrate the technical aspects of the method. Next, an observer study using visual grading characteristics is performed to analyze the diagnostic implications of motion compensation in a series of lower extremity CBCT scans with moderate to severe motion.

Materials and Methods

Patient population and CBCT imaging protocols

In this IRB-approved, HIPPA-compliant study, we retrospectively reviewed the CBCT images of 154 patients who had undergone both WB and non-weight-bearing (NWB) scans of lower extremity as a part of clinical feasibility study of extremity CBCT (see Figure 1). These patients were referred based on a wide variety of symptoms including knee, ankle and foot pain. Three hundred and eight WB and NWB CBCT images of these 154 patients were reviewed by a fellowship-trained musculoskeletal radiologist to identify images with significant motion artifact. In this study, we only included images with moderate to severe motion artifact which prevented optimal assessment of osseous and soft-tissue structures. A total of 24 scans of 22 subjects (18 male, 4 female, mean 32 years of age, range 21-74 years of age) were chosen for inclusion in the study (Figure 1). The majority of the motion-contaminated datasets (22 out of 24) was from weight-bearing acquisitions. Two study subjects had motion in both the WB and NWB conditions, thus, two scans were included in the study for those two subjects.

The images were acquired on a clinical prototype of the Carestream OnSight 3D extremity CBCT system (Carestream Health, Rochester NY), using a research protocol based on previous technical assessment [6]. The OnSight 3D system implements a multi-source x-ray generator to reduce the impact of the so-called cone-beam artifacts [17]. Such artifacts are associated with incomplete sampling of axial planes above and below the central slice and manifest as distortions of features that are perpendicular to the axis of rotation (e.g. articular surfaces). Three x-ray tubes are arranged along a vertical line parallel to the axis of rotation, so that each source compensates the regions of poor sampling of its neighbor. The data from the three sources are combined during the reconstruction using a spatial weighting scheme, minimizing cone-beam artifacts [17]. The scan time was ~20 sec. The X-ray tubes were operated at 80 kV, total scan mAs was 108 mAs, and the imaging dose was 15 mGy [5]. The NWB scan was performed in a sitting position with the imaged joint placed within the CBCT gantry and the WB scan was performed with the patient standing with feet approximately at shoulder width, distributing their weight evenly between both lower extremities. In both configurations, only one joint was imaged at a time, with the other extremity remaining outside of the scanner bore and the irradiated field of view. Reconstruction protocol involved Feldkamp filtered back projection (FBP) with sharp (bone) and smooth (soft-tissue) kernels, each with 0.56 mm isotropic voxels.

Motion compensation algorithm

The motion compensation algorithm, including mathematical details, was introduced in a previous technical publication [14]. Here we provide a brief summary of the method, illustrated by an experimental CBCT study with an anthropomorphic phantom and a controlled motion pattern.

The motion trajectory T is modeled as a time-dependent sequence of rigid transformations of the object. Each rigid transformation involves six degrees of freedom, that is three translations (two in the axial plane and one in the longitudinal plane) and three rotations

(both in and out of the axial plane). Because the CBCT geometry simultaneously acquires data in all three dimensions (as opposed to conventional spiral CT, where the slices are imaged at different time points), the compensation algorithm can estimate motions that occur out of the axial plane. For any given trajectory, a motion-compensated reconstruction is obtained by applying the sequence T in the backprojection step of image reconstruction. Since the trajectory of patient motion is not known *a priori*, one needs to estimate it from scan data. We employ the concept of autofocus: since uncompensated patient motion causes blur (unsharpness) in the reconstructed image, the motion trajectory can be found through an optimization procedure that evolves an initial guess for the sequence T until sharpness is maximized in the compensated image. As long as projection data is available, this procedure can be applied retrospectively when motion artifacts are present in the initial reconstruction.

We use variance of image gradient (VIG) as the sharpness metric and a stochastic iterative optimization technique [18] for maximization. The method is implemented in Matlab (Mathworks, Natick MA) with GPU parallelization.

In this study, the VIG used for compensation was computed over a user-selected Region of Interest (ROI) and the resulting T was applied to the whole reconstructed volume under the assumption that the entire extremity underwent the same rigid motion (e.g. a global shift and/or rotation). Alternatively, the method can be run in separate local ROIs (e.g., distal femur and proximal tibia) in cases where the motion is not globally rigid – e.g., flexion or extension [19].

Tunable parameters of the algorithm include ROI size and location, and regularization strength controlling unrealistic abrupt motion estimates. Previous technical assessment indicated that the performance of compensation depends only weakly on such parameters (11) and that they can be set based on a rough visual assessment of motion characteristics in motion-contaminated reconstruction. This approach was used in this work, recognizing that future studies will be needed to fully automate parameter selection.

The compensation was applied retrospectively in an offline fashion. The runtime of the method depends on the complexity of the motion pattern and is therefore case-specific. In the current unoptimized computer implementation of the algorithm, the compensation times for the datasets considered in this study varied between ~10 min and ~50 min. These runtimes are comparable to those previously reported for phantom experiments in [14].

The performance of the algorithm under controlled motion, including comparison against a static image of the same object, is illustrated in an experiment in Figure 2. An anthropomorphic knee phantom (The Phantom Laboratory, Salem NY) was imaged in the extremity CBCT using the same acquisition protocol as in the clinical study. The base of the phantom was immobilized and a translation stage provided controlled step motion of prescribed amplitude (1-5 mm) to the top of the phantom (Figure 2A). The top row of Figure 2B shows a reconstruction of the phantom acquired under a static condition, as well as uncompensated images with motion. Typical motion artifact patterns are apparent, including image blur that increases with motion severity. The motion-induced blur is captured by VIG (Figure 2C), which is 16% - 24% lower from that of the static volume and decreases as a

function of motion amplitude (VIG is higher for sharper images). The VIG was computed within a “motion compensation ROI” indicated by a dashed box in the image of a static phantom. The bottom row of Figure 2B shows motion compensated images obtained by maximizing the VIG of the ROI. Reduction of artifacts is accompanied by increased VIG (as expected in a VIG-maximizing algorithm), which is restored to values within 10% of the static volume independent of the motion amplitude. This illustrates the link between image sharpness and motion artifact reduction that underlies the autofocus approach. The motion amplitudes estimated by the algorithm agree with those actually imparted by the motion system (Figure 2D). Slight deviations between the estimated and actual motion resulted in minor residual artifacts.

Further technical performance evaluation of the compensation algorithm against motion-free ground truth can be found in [14]. Simulations and experiments with anthropomorphic phantoms showed a clear reduction of motion artifacts for a broad range of motion amplitudes (0.5 mm to 10 mm). The agreement between the reconstruction of a motion-contaminated scan and a static image of the same object was substantially improved after the compensation, as evidenced by ~70% increase in the structural similarity index (SSIM) across the range of motion amplitude included in the study.

Qualitative assessment

Assessment of all images was performed independently by three observers: a musculoskeletal radiologist with eight years of experience; and two musculoskeletal radiology fellows with four and two years of experience in interpretation of musculoskeletal CT images. Readings were conducted using diagnostic quality monitors calibrated to DICOM standards. Four tasks were selected based on the ability to visualize 1) cortical bone, 2) trabecular bone, 3) joint space, and 4) patellar or Achilles tendon (depending on body site). The tasks were scored by the three observers based on a nine-level Likert scale [5] and assigned numerical scores as shown in Table 1. Score of 5 (“Excellent”) indicates diagnostic quality without any artifacts; score of 4 (“Good”) indicates diagnostic quality with minor artifacts; score of 3 (“Fair”) corresponded to adequate visualization with moderate artifacts; images scored as 2 and 1 (“Poor” and “Very Poor”) were non-diagnostic. In addition to the visualization tasks, artifact reduction throughout the field of view was also scored using the Likert scale (1-severe artifacts, 2- moderate to severe, 3-moderate artifacts, 4-mild artifacts, 5-no artifacts).

Scores were recorded for the original CBCT images with motion artifacts and the motion compensated images presented in randomized reading order and with observers blinded to whether motion compensation had been applied. Reconstructions obtained with the bone kernel were used for scoring the cortical and trabecular tasks. All other tasks were evaluated in soft tissue images. In total, 96 datasets (24 patients, 2 reconstruction kernels, with and without compensation) were reviewed.

Statistical Analysis

Inter-observer agreement was assessed using intra-class correlation coefficient (ICC) employing PAWS (V.20, Chicago, IL). ICC values higher than 0.74 were regarded as

excellent agreement between readers, values between 0.6 and 0.74 indicated good agreement, values between 0.4 and 0.59 were interpreted as fair agreement, and ICC values lower than 0.4 were considered poor correlation [20].

A non-parametric rank-invariant statistical data analysis method called visual grading characteristic (VCG) was utilized to establish the effects of motion compensation on expert observer performance in clinical tasks. Following the previously described methodology [21], the mentioned diagnostic satisfaction scale was further stratified. For each image and task, a mean score of the three observers was used to assign a grade on the stratified scale for that task. The next step involved building a table describing the percentage of observations (images) that achieved a satisfaction score equal to or lower than a certain value [4, 21]. Those fractions will be referred to as image criteria scores (ICS). For instance, an ICS score of Z%for “poor” diagnostic satisfaction indicated that Z% of all observations of a task were scored as “poor” to “very poor”, while the remaining (100-Z%) had a grade of “fair” to “excellent”. Two ICS tables were obtained, one for the original (uncompensated) reconstructions, and one for motion compensated images. The resulting pairs of ICS values were analyzed using the ROCKIT software package (C E Metz, University of Chicago) to generate a continuous VGC curve and to calculate the area under the curve (AUC_{VGC}) [4, 21]. The AUC_{VGC} is a relative measure of image quality as indicated by the diagnostic satisfaction scale.

Results

The interobserver agreement of the diagnostic satisfaction scores was excellent for all five categories before (ICC range 0.77-0.90) and after motion correction (ICC range 0.89-0.95).

Table 2 summarizes the distribution of mean observer ratings for all visualization tasks. Because of the averaging, the scores in this and the following table are more finely stratified than those used by the raters (Table 1). The number of images that achieved certain mean score (on the stratified scale) is compared for the original (O) and motion compensated (M) populations. Table 3 shows the pairs of ICS datapoints (original vs. compensated) obtained from Table 2. For instance, in terms of cortical bone, before motion compensation, 41.7% of images were scored as poor or very poor, as opposed to only 8.3% of observations following motion compensation. Without motion compensation, the fraction of images scored “Poor” or “Very Poor” varied between 25% for tendon to over 40% for bone tasks, which are particularly sensitive to image sharpness. After compensation, the fraction of images scored “Poor” or “Very Poor” was reduced to less than 10% across all tasks. In terms of artifact severity, 100% (24/24) of cases were found to exhibit moderate to severe artifacts (scores of “Fair” and worse) without compensation, compared to only 37.5% (9/24) scans after compensation. Analysis of these datapoints yielded the results on the VCG curve displayed in Figure 3 as well as the AUC_{VGC} values and their 95% confidence intervals (CI), displayed in Table 4. The results of VGC analysis indicate the favorability of images following motion compensation when compared with original images across all visualization task. The lower bound CI is above 0.5 for all tasks, confirming statistically significant improvement in diagnostic satisfaction after motion compensation (AUC_{VGC} of 0.78 to 0.88). The lowest

value of AUC_{VGC} was found in tendons, likely reflecting known challenges in soft-tissue visualization that affect diagnostic performance of CBCT even without motion [5].

Figure 4 compares uncompensated and motion-compensated patient images for two cases, one with motion amplitude (as estimated by the compensation algorithm) of 3.1 mm and one with motion amplitude of 31.8 mm, representing the most severe motion encountered in the patient cohort. The improvement in visualization of the anatomy is displayed in the lower row of images. It is worth noting that the compensation algorithm reduced the streaks emanating from the articular surfaces of the knee (as seen in the sagittal view in Fig. 4A), which resemble typical patterns of the cone-beam artifact. However, such distortions might also be caused by motion and thus correctable by our approach. This was likely the case in this dataset, since the cone-beam effects had been minimized by means of the multi-source configuration of the scanner and because the knee was placed close to the central plane of the central x-ray tube.

Discussion

The study demonstrates that autofocus-based motion compensation substantially improves the diagnostic quality of extremity CBCT scans affected by motion [14]. We note that the overall incidence of moderate to severe motion artifact in the population of over 300 lower extremity scans was less than 10% (24/308); when considering only WB acquisitions, the frequency of artifacts was 14% (22/154). This observation indicates that the light immobilization employed during scanning provides a reasonable degree of robustness to motion. However, efficient compensation algorithms are essential for extremity CBCT since motion artifacts, when present, often render the images non-diagnostic and thus incur additional radiation dose (if a repeat scan is needed) and time.

The autofocus-based approach is purely retrospective and requires no hardware modifications or prior data. This confers significant advantages in clinical workflow compared to other algorithms for compensation of non-periodic motions, which often rely on fiducials [15, 16] or require a motion-free prior CT to enable 2D/3D registration [22, 23]. It is important to note that our earlier technical evaluation of the algorithm showed that the autofocus algorithm does not introduce any spurious structures during motion compensation, i.e. the resulting image agrees well with a motion-free reconstruction of the same object [14]. More specifically, we investigated structural similarity index (SSIM) between autofocus-compensated reconstructions and motion-free scans of the same phantom. SSIM values of ≥0.8 were found across a range of phantoms and motion amplitudes.

The algorithm uses a stochastic optimizer that involves repeated reconstructions of the ROI using an evolving population of motion estimates. Despite the large number of reconstructions involved (typically ~30,000 per case), the process can be efficiently executed using parallel computing capabilities of modern GPUs. The currently unoptimized, research-only implementation of the algorithm incurs a runtime of ~10 - 50 min per case, depending on the motion amplitude. The runtime could be reduced to 1-5 min using multiple GPUs and a more optimized implementation.

Currently, there is no established protocol for clinical review of motion compensated datasets. We anticipate that the initial implementation of this method in radiological practice might involve presenting the reader with both the original and the corrected images. Such a comparison will help establish confidence in the compensation by enabling the radiologist to critically evaluate the effects of the algorithm and determine whether any remaining image distortions are due to uncompensated motion or other sources.

We acknowledge several limitations of our study. Despite the relatively large population of over 300 scans, only 24 cases met the inclusion criteria for this technical note, i.e. moderate to severe motion artifact. The criteria were chosen to focus performance evaluation on conditions where motion compensation was essential to restore diagnostic image quality. However, the resulting sample size was relatively small. Nevertheless, the cohort was sufficient to demonstrate the feasibility of improving diagnostic satisfaction in presence of motion. A larger sample would enable additional analysis, including stratification of results by motion amplitude.

The results of our observer study show that the autofocus algorithm improves diagnostic satisfaction in CBCT scans that were originally considered non-diagnostic due to motion artifacts. The VGC analysis confirmed noticeable reduction of artifacts and substantially improved visualization of trabecular details and bone boundaries following motion compensation. The autofocus algorithm could thus provide a valuable tool in the growing practice of musculoskeletal CBCT imaging. The method also has potential application beyond CBCT in correction of residual artifacts in dynamic imaging of the joints [24, 25].

Acknowledgments

Funding: This research was supported by NIH grant R01-EB-018896, collaboration with the US Army NSRDEC (grant W911QY-14-C-0014), and Carestream Health.

Abbreviation:

CBCT	Cone Beam CT
MDCT	Multi-detector CT
HIPPA	Health Insurance Portability and Accountability Act
VIG	Variance Of Image Gradient
ROI	Region of Interest
ICS	Image Criteria Scores
ICC	Intraclass Correlation
VGC	Visual Grading Characteristics

References:

1. Pugmire BS, Shailam R, Sagar P, Liu B, Li X, Palmer WE, et al. Initial Clinical Experience With Extremity Cone-Beam CT of the Foot and Ankle in Pediatric Patients. AJR American journal of roentgenology. 2016; 206(2):431–435. [PubMed: 26797374]
2. Shakoor D, Osgood GM, Brehler M, Zbijewski WB, de Cesar Netto C, Shafiq B, et al. Cone-beam CT measurements of distal tibio-fibular syndesmosis in asymptomatic uninjured ankles: does weight-bearing matter? Skeletal radiology. 2018.
3. Lintz F, de Cesar Netto C, Barg A, Burssens A, Richter M. Weight-bearing cone beam CT scans in the foot and ankle. EFORT open reviews. 2018; 3(5):278–286. [PubMed: 29951267]
4. Osgood GM, Thawait GK, Hafezi-Nejad N, Shakoor D, Shaner A, Yorkston J, et al. Image quality of cone beam computed tomography for evaluation of extremity fractures in the presence of metal hardware: visual grading characteristics analysis. The British journal of radiology. 2017; 90(1073): 20160539. [PubMed: 28281784]
5. Demehri S, Muhit A, Zbijewski W, Stayman JW, Yorkston J, Packard N, et al. Assessment of image quality in soft tissue and bone visualization tasks for a dedicated extremity cone-beam CT system. European radiology. 2015; 25(6):1742–1751. [PubMed: 25599933]
6. Carrino JA, Al Muhit A, Zbijewski W, Thawait GK, Stayman JW, Packard N, et al. Dedicated cone-beam CT system for extremity imaging. Radiology. 2014; 270(3):816–824. [PubMed: 24475803]
7. de Cesar Netto C, Schon LC, Thawait GK, da Fonseca LF, Chinanuvathana A, Zbijewski WB, et al. Flexible Adult Acquired Flatfoot Deformity: Comparison Between Weight-Bearing and Non-Weight-Bearing Measurements Using Cone-Beam Computed Tomography. The Journal of bone and joint surgery American volume. 2017; 99(18):e98. [PubMed: 28926392]
8. Thawait GK, Demehri S, AlMuhit A, Zbijweski W, Yorkston J, Del Grande F, et al. Extremity cone-beam CT for evaluation of medial tibiofemoral osteoarthritis: Initial experience in imaging of the weight-bearing and non-weight-bearing knee. European journal of radiology. 2015; 84(12):2564–2570. [PubMed: 26388464]
9. Sisniega A, Zbijewski W, Badal A, Kyprianou IS, Stayman JW, Vaquero JJ, et al. Monte Carlo study of the effects of system geometry and antiscatter grids on cone-beam CT scatter distributions. Medical physics. 2013; 40(5):051915. [PubMed: 23635285]
10. Sisniega A, Zbijewski W, Xu J, Dang H, Stayman JW, Yorkston J, et al. High-fidelity artifact correction for cone-beam CT imaging of the brain. Physics in medicine and biology. 2015; 60(4): 1415–1439. [PubMed: 25611041]
11. Zbijewski W, Sisniega A, Stayman JW, Muhit A, Thawait G, Packard N, et al. High-Performance Soft-Tissue Imaging in Extremity Cone-Beam CT. Proceedings of SPIE--the International Society for Optical Engineering. 2014; 9033:903329. [PubMed: 25076825]
12. Siewerdsen JH. Cone-Beam CT with a Flat-Panel Detector: From Image Science to Image-Guided Surgery. Nuclear instruments & methods in physics research Section A, Accelerators, spectrometers, detectors and associated equipment. 2011; 648(Sl):S241–s250.
13. Lang H, Neubauer J, Fritz B, Spira EM, Strube J, Langer M, et al. A retrospective, semi-quantitative image quality analysis of cone beam computed tomography (CBCT) and MSCT in the diagnosis of distal radius fractures. European radiology. 2016; 26(12):4551–4561. [PubMed: 27003138]
14. Sisniega A, Stayman JW, Yorkston J, Siewerdsen JH, Zbijewski W. Motion compensation in extremity cone-beam CT using a penalized image sharpness criterion. Physics in medicine and biology. 2017; 62(9):3712–3734. [PubMed: 28327471]
15. Choi JH, Fahrig R, Keil A, Besier TF, Pal S, McWalter EJ, et al. Fiducial marker-based correction for involuntary motion in weight-bearing C-arm CT scanning of knees. Part I. Numerical model-based optimization. Medical physics. 2013; 40(9):091905. [PubMed: 24007156]
16. Choi JH, Maier A, Keil A, Pal S, McWalter EJ, Beaupre GS, et al. Fiducial marker-based correction for involuntary motion in weight-bearing C-arm CT scanning of knees. II. Experiment. Medical physics. 2014; 41(6):061902. [PubMed: 24877813]

17. Gang GJ, Zbijewski W, Mahesh M, Thawait G, Packard N, Yorkston J, et al. Image quality and dose for a multisource cone-beam CT extremity scanner. Medical physics. 2018; 45(1):144–155. [PubMed: 29121409]

18. Hansen N, Muller SD, Koumoutsakos P. Reducing the time complexity of the derandomized evolution strategy with covariance matrix adaptation (CMA-ES). Evolutionary computation. 2003; 11(1):1–18. [PubMed: 12804094]

19. Sisniega AWZPW, Stayman JW, Aygun N, Stevens R, Wang X, Foos DH, Siewerdsen JH,. Multi-Motion Compensation for High-Quality Cone-Beam CT of the Head The Fifth International Conference on Image Formation in X-Ray Computed Tomography, Salt Lake City, UT 2018.

20. Fleiss JL. Statistical methods for rates and proportions. Wiley, John and Sons, Inc, New York, NY 1981.

21. Bath M, Mansson LG. Visual grading characteristics (VGC) analysis: a non-parametric rank-invariant statistical method for image quality evaluation. The British journal of radiology. 2007; 80(951):169–176. [PubMed: 16854962]

22. Berger M, Müller K, Aichert A, Unberath M, Thies J, Choi JH, et al. Marker-free motion correction in weight-bearing cone-beam CT of the knee joint. Medical physics. 2016; 43(3):1235–1248. [PubMed: 26936708]

23. Ouadah S, Jacobson M, Stayman J, Ehtiati T, Weiss C, Siewerdsen J. Correction of patient motion in cone-beam CT using 3D–2D registration. Physics in Medicine & Biology. 2017; 62(23):8813. [PubMed: 28994668]

24. Demehri S, Hafezi-Nejad N, Morelli JN, Thakur U, Lifchez SD, Means KR, et al. Scapholunate kinematics of asymptomatic wrists in comparison with symptomatic contralateral wrists using four-dimensional CT examinations: initial clinical experience. Skeletal radiology. 2016; 45(4): 437–446. [PubMed: 26659662]

25. Demehri S, Wadhwa V, Thawait GK, Fattahi N, Means KR, Carrino JA, et al. Dynamic evaluation of pisotriquetral instability using 4-dimensional computed tomography. Journal of computer assisted tomography. 2014; 38(4):507–512. [PubMed: 24834894]

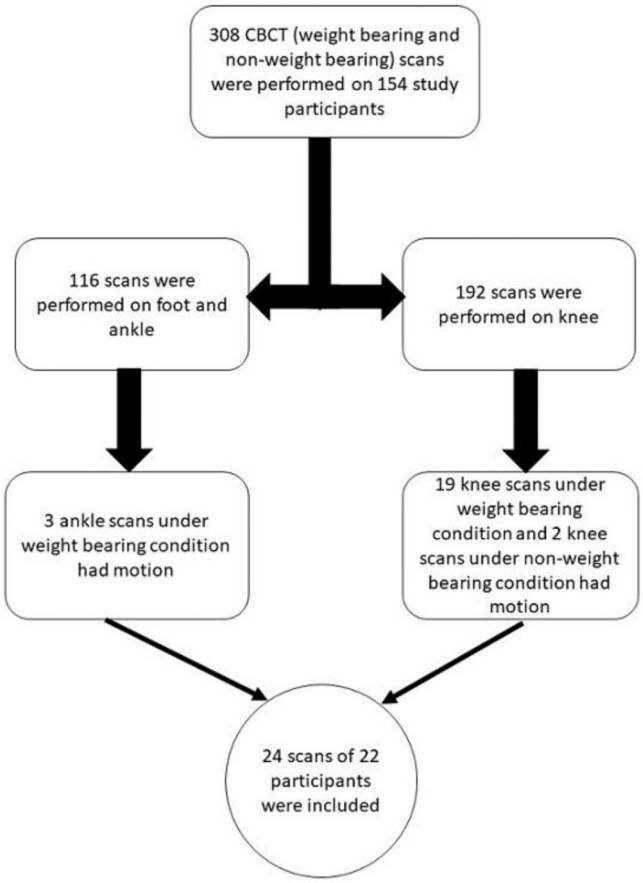

Figure 1.
Flowchart for retrospective cases selection in this study.

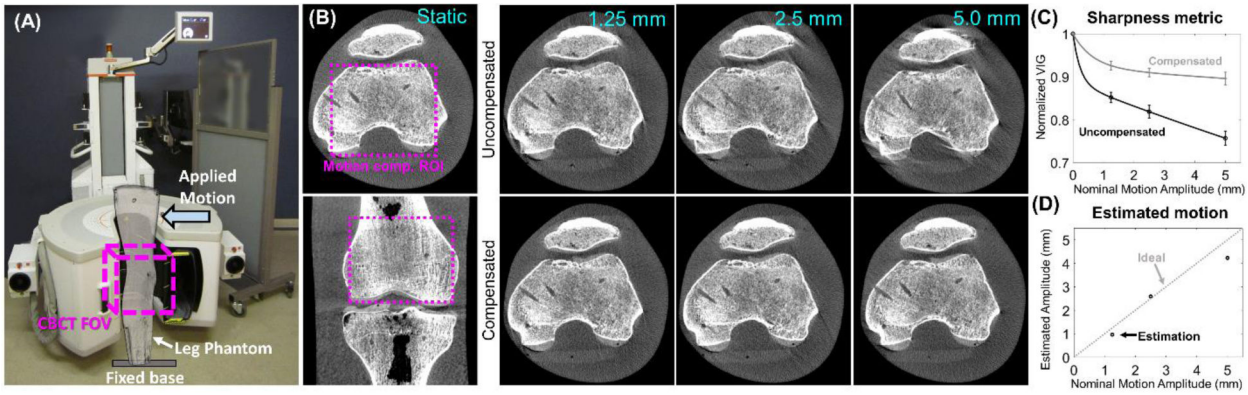

Figure 2.

2A. Extremity CBCT scanner in the configuration for imaging of lower extremities and the experimental setup for the phantom study. 2B, top row: uncompensated reconstructions of the phantom for a range of motion amplitudes. Typical features of motion artifact are present. 2B, bottom row: motion compensated reconstructions. Reduction in artifacts is apparent. 2C: the image sharpness metric VIG as a function of motion amplitude for reconstructions with and without compensation. 2D: Motion amplitude estimated by the compensation algorithm is compared to nominal amplitude prescribed in the experiment.

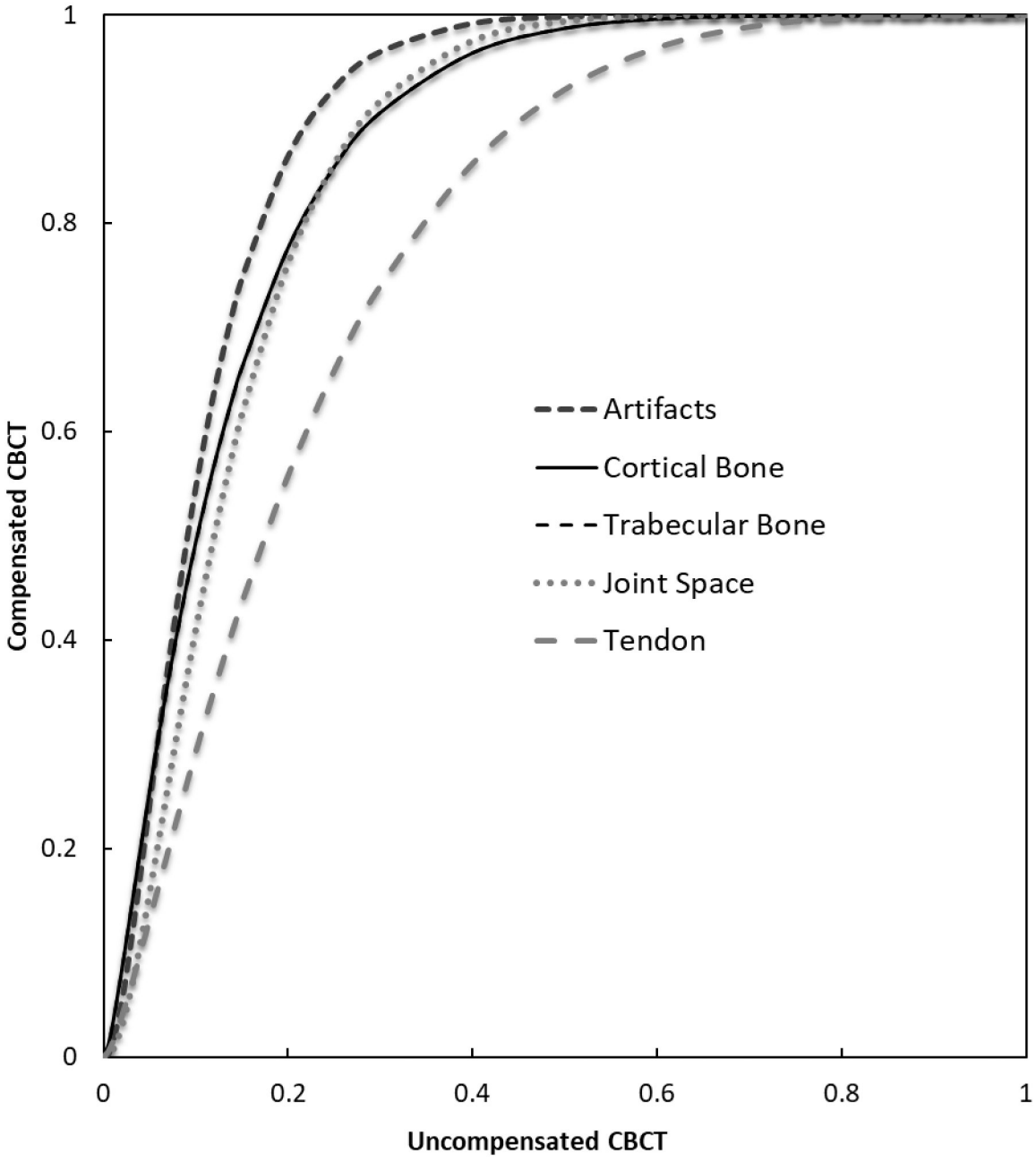

Figure 3.

Visual grading characteristic analysis for visualization tasks. Motion compensated Cone-Beam CT (CBCT) is displayed in y-axis and original uncompensated CBCT is displayed in x-axis. The curves demonstrate the preference for motion compensated CBCT images for all tasks.

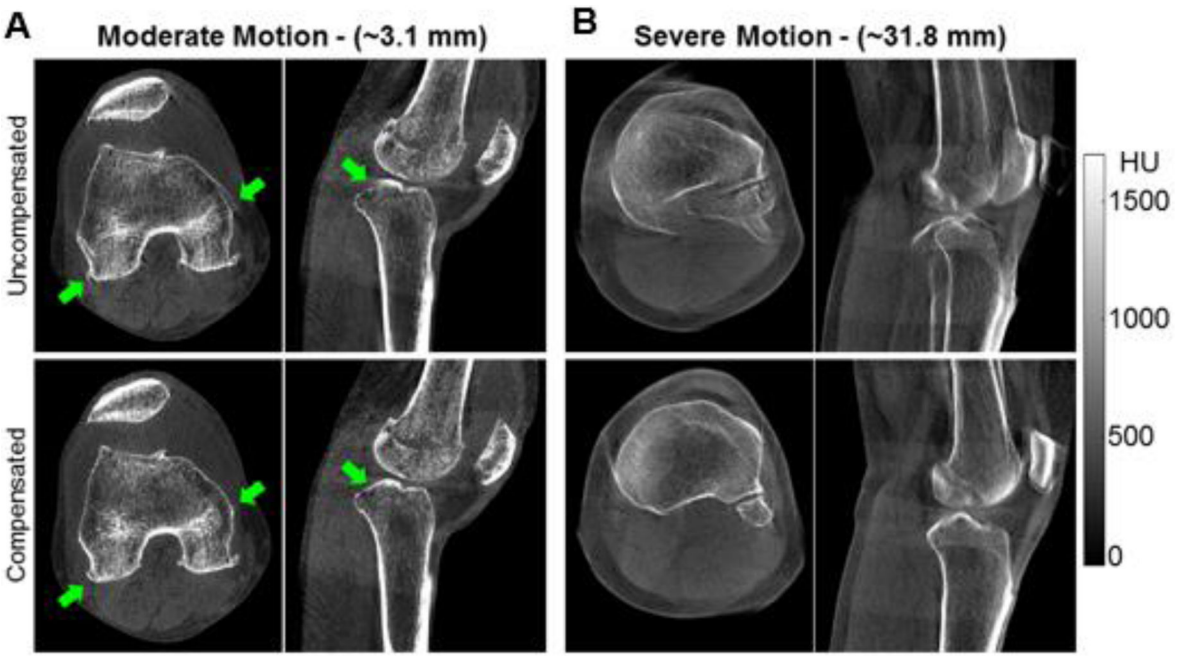

Figure 4.
Comparison of patient images before and after motion correction.

Table 1.

Details of the diagnostic satisfaction scale for the assessment of the visualization tasks.

Score	Visibility	Ability to Assess	Interpretation
5	Excellent	Excellent	Diagnostic quality, without any artifacts
4.50	Indecisive between Good and Excellent		
4	Good	Good	Diagnostic quality, with minor artifacts
3.5	Indecisive between Fair and Good		
3	Fair	Adequate	Diagnostic quality, with moderate artifacts identified
2.5	Indecisive between Fair and Poor		
2	Poor	Challenging	Non-diagnostic quality, the visualization task can be identified
1.5	Indecisive between Very Poor and Poor		
1	Very Poor	Very Challenging	Non-diagnostic quality, the visualization task cannot be identified

Table 2.

Count of average observer ratings for the five visualization tasks.

Score	Cortical Bone		Trabecular Bone		Joint Space		Patellar Tendon		Artifacts	
	O	M	O	M	O	M	O	M	O	M
1:very poor	3	1	4	1	3	1	2	1	3	1
1.17	0	0	0	0	0	0	0	0	0	0
1.33	0	0	0	0	0	0	0	0	0	0
1.5	0	0	0	0	0	0	0	0	0	0
1.67	2	0	0	0	0	0	0	0	0	0
1.83	0	0	0	0	0	0	0	0	0	0
2: Poor	5	1	6	1	4	1	4	1	7	1
2.17	0	0	5	0	5	0	5	1	5	0
2.33	2	0	0	0	0	0	1	0	0	0
2.5	4	2	3	2	4	2	3	3	4	1
2.67	0	0	0	0	0	0	2	0	1	0
2.83	3	0	0	1	0	0	0	1	0	1
3 : Fair	4	5	5	5	7	6	6	8	3	5
3.17	0	0	0	0	1	0	1	1	0	0
3.33	0	1	0	0	0	0	0	0	0	0
3.5	0	1	0	1	0	1	0	2	0	1
3.67	0	0	0	0	0	0	0	0	0	0
3.83	0	0	1	1	0	0	0	1	1	0
4: Good	1	7	0	9	0	9	0	5	0	13
4.17	0	0	0	0	0	0	0	0	0	0
4.33	0	0	0	0	0	1	0	0	0	0
4.5	0	0	0	1	0	1	0	0	0	1
4.67	0	1	0	0	0	2	0	0	0	0
4.83	0	1	0	0	0	0	0	0	0	0
5:Excellent	0	4	0	2	0	0	0	0	0	0

O: Original

M: Motion compensated

Table 3.

Pairs of Image Criteria Scores (ICS) for each task.

Score	Cortical Bone		Trabecular Bone		Joint Space		Tendon		Artifacts	
	O	M	O	M	O	M	O	M	O	M
1:Very Poor	12.5	4.2	16.7	4.2	12.5	4.2	8.3	4.2	12.5	4.2
1.17	12.5	4.2	16.7	4.2	12.5	4.2	8.3	4.2	12.5	4.2
1.33	12.5	4.2	16.7	4.2	12.5	4.2	8.3	4.2	12.5	4.2
1.5	12.5	4.2	16.7	4.2	12.5	4.2	8.3	4.2	12.5	4.2
1.67	20.8	4.2	16.7	4.2	12.5	4.2	8.3	4.2	12.5	4.2
1.83	20.8	4.2	16.7	4.2	12.5	4.2	8.3	4.2	12.5	4.2
2: Poor	41.7	8.3	41.7	8.3	29.2	8.3	25.0	8.3	41.7	8.3
2.17	41.7	8.3	62.5	8.3	50.0	8.3	45.8	12.5	62.5	8.3
2.33	50.0	8.3	62.5	8.3	50.0	8.3	50.0	12.5	62.5	8.3
2.5	66.7	16.7	75.0	16.7	66.7	16.7	62.5	25.0	79.2	12.5
2.67	66.7	16.7	75.0	16.7	66.7	16.7	70.8	25.0	79.2	12.5
2.83	79.2	16.7	75.0	20.8	66.7	16.7	70.8	29.2	83.3	16.7
3 : Fair	95.8	37.5	95.8	41.7	95.8	41.7	95.8	62.5	95.8	37.5
3.17	95.8	37.5	95.8	41.7	100	41.7	100	66.7	95.8	37.5
3.33	95.8	41.7	95.8	41.7	100	41.7	100	66.7	100	37.5
3.5	95.8	45.8	95.8	45.8	100	45.8	100	75.0	100	41.7
3.67	95.8	45.8	95.8	45.8	100	45.8	100	75.0	100	41.7
3.83	95.8	45.8	100	50.0	100	45.8	100	79.2	100	41.7
4: Good	100	75.0	100	87.5	100	83.3	100	100	100	95.8
4.17	100	75.0	100	87.5	100	83.3	100	100	100	95.8
4.33	100	75.0	100	87.5	100	87.5	100	100	100	95.8
4.5	100	75.0	100	91.7	100	91.7	100	100	100	100
4.67	100	83.3	100	91.7	100	100	100	100	100	100
4.83	100	100	100	91.7	100	100	100	100	100	100
5:Excellent	100	100	100	100	100	100	100	100	100	100

O: Original

M: Motion compensated

Table 4.

Area Under the Curve derived from Visual Grading Characteristics (VGC) curves (AUC_{VGC}). All visualization tasks were significantly in favor of motion compensated images.

Score	Cortical bone	Trabecular bone	Joint Space	Tendon	Artifacts
AUC_{VGC}	0.8659	0.8658	0.8568	0.7846	0.8883
95% CI Lower bound	0.7309	0.7299	0.7129	0.6313	0.7545
95% CI Upper bound	0.9451	0.9453	0.9418	0.8926	0.9596

CI: Confidence Interval